

Navier-Stokes Flow Field Analysis of
Compressible Flow in a High Pressure Safety Relief Valve

Bruce Vu and Ten-See Wang
Computational Fluid Dynamics Branch
NASA Marshall Space Flight Center

Ming-Hsin Shih and Bharat Soni
Engineering Research Center for Computational Field Simulation
Mississippi State University

Abstract

The objective of this study is to investigate the complex three-dimensional flowfield of an oxygen safety pressure relieve valve during an incident, with a computational fluid dynamics (CFD) analysis. Specifically, the analysis will provide a flow pattern that would lead to the explanation of the eventual erosion pattern of the hardware, so as to combine it with other findings to piece together a most likely scenario for the investigation. The CFD model is a pressure based solver. An adaptive upwind difference scheme is employed for the spatial discretization, and a predictor, multiple corrector method is used for the velocity-pressure coupling. The computational result indicated vortices formation near the opening of the valve which matched the erosion pattern of the damaged hardware.

Introduction

On Friday, August 28, 1992, there was a fire on Test Stand 116 at the location of a high pressure Safety Relieve Valve (SRV)-9391. An investigation team was formed and a timeline based upon recorded valve opening and closing times and personnel observations was developed. This timeline, the hardware inspections, and analyses led the team to believe two anomalies occurred. The first was the inadvertent pressurization of the Liquid Oxidizer (LOX) tank which resulted in, second, a fire in SRV-9391 during high pressure LOX discharge. An extensive fault tree was developed related to both of these anomalies. One of the task assigned to the personnel of Computational Fluid Dynamics (CFD) branch was to investigate the flow pattern that occurred during the inadvertent opening of the valve, so as to understand what may have happened during the incident.

Fig. 1 shows a general arrangement of the pilot operated SRV. The valve inlet is connected to the LOX tank. The pilot valve is used to regulate the actuation pressure of the main valve system. The SRV consists of a main cylinder and a piston, with a smaller diameter inlet. The valve is designed to open when the line pressure reaches 5500 psi. That is, the piston will be lifted and

the LOX will be flowing through the nozzle and escape to a dump container or the ambient. Fig. 2 shows the valve body after the mishap. On the right is what was left of the original valve seating, the erosion pattern that indicated a swirling flame propagation can be seen, while on the left is what was left of the original valve outlet connection. In order to fully understand the flow anomaly, a three-dimensional CFD analysis was carried out to investigate the flow pattern inside SRV during the incident.

Governing Equations

The basic equations employed to describe the SRV flowfield are the multi-dimensional, general coordinate transport equations. A generalized form of these equations written in curvilinear coordinates is given by

$$(1/J)(\partial \rho q / \partial t) = \partial [-\rho U_i q + \mu G_{ij} (\partial q / \partial \xi_j)] / \partial \xi_i + (1/J) S_q$$

where J , U_i and G_{ij} are written as:

$$J = \partial(\xi_i, \xi_j) / \partial(x, y)$$

$$U_i = (u_j / J) (\partial \xi_i / \partial x_j)$$

$$G_{ij} = (\partial \xi_i / \partial x_k) (\partial \xi_j / \partial x_k) / J$$

q represents $1, u, v, w, h, k,$ and ϵ , respectively. These are equations of continuity, x, y and z momentum, enthalpy, turbulent kinetic energy, and turbulent kinetic energy dissipation rate. ξ is the transformed curvilinear coordinate. $\mu = (\mu_l + \mu_t) / \sigma_q$ is the effective viscosity when the turbulent eddy viscosity concept is employed to model the turbulent flows. μ_l is the laminar viscosity; $\mu_t = \rho C_\mu k^2 / \epsilon$, is the turbulence eddy viscosity and C_μ and σ_q denote turbulence modeling constants. Turbulence modeling constants σ_q and source terms S_q are given in Table 1.

Table 1 σ_q and S_q of the transport equations

q	σ_q	S_q
1	1.00	0
u	1.00	$-\rho p_x + \nabla[\mu(u_j)_x] - 2/3(\mu \nabla u_j)_x$
v	1.00	$-\rho p_y + \nabla[\mu(u_j)_y] - 2/3(\mu \nabla u_j)_y$
w	1.00	$-\rho p_z + \nabla[\mu(u_j)_z] - 2/3(\mu \nabla u_j)_z$
h	0.95	$Dp/Dt + \Phi$
k	0.89	$\rho(P_r - \epsilon)$
ϵ	1.15	$\rho(\epsilon/k)(C_1 P_r - C_2 \epsilon + C_3 P_r^2 / \epsilon)$

Where Φ is the energy dissipation function, P_r represents the turbulent kinetic energy production term. C_1 , C_2 and C_3 are model constants for the two-equation turbulence model. Homogeneous flow approach is adopted in case of phase changes.

Numerical Schemes

To solve the system of nonlinear coupled partial differential equations, finite difference approximations are used to establish a system of linearized algebraic equations. A relaxation solution procedure is then employed to couple the equations. An adaptive upwind scheme was employed to approximate the convective terms of the momentum, energy and continuity equations; the scheme is based on second and fourth order central differencing with artificial dissipation. First order upwinding is used for species and turbulence equations, since the parameters involved are positive quantities. Different eigenvalues are used for weighing the dissipation terms depending on the conserved quantity being evaluated, in order to give correct diffusion fluxes near wall boundaries. Adding the dissipation term to the convective fluxes F in computational coordinate ξ produces

$$\partial F / \partial \xi = (F_{i+1} - F_{i-1}) / 2 - (D_{i+1/2} - D_{i-1/2})$$

The dissipation term, D , is constructed such that a fourth-order central and fourth-order damping scheme is activated in smooth regions, and a second-order central and second-order damping scheme is used near shock waves. Since the Jacobian matrices of the Euler fluxes have eigenvalues of U , $U+a$ (a is the speed of sound) and $U-a$, it is sufficient to use the magnitudes of these eigenvalues to weigh the dissipation terms to maintain the smoothness of the solution without losing accuracy. $|U|+a$ was used for the continuity equation and $|U|$ was used for other transport equations. General forms of the dissipation terms are given by: for the continuity equations,

$$D_{i+1/2} = D_1 (\rho_{i+1} - \rho_i) + D_2 (\rho_{i-1} - 3\rho_i + 3\rho_{i+1} - \rho_{i+2})$$

and for other transport equations,

$$D_{i+1/2} = D_3 (q_{i+1} - q_i) + D_4 (q_{i-1} - 3q_i + 3q_{i+1} - q_{i+2}) \\ + (1-\epsilon_1) (\rho U_{i+1/2} / 16) [(q_i - q_{i-1}) - (q_{i+2} - q_{i+1})]$$

where

$$D_1 = 0.25 v_{i+1/2} (|U|+a)_{i+1/2}$$

$$D_2 = \text{MAX}\{0, 0.01 - 0.25 v_{i+1/2}\} (|U|+a)_{i+1/2}$$

$$D_3 = 0.5 \epsilon_1 |\rho U|_{i+1/2}$$

$$D_4 = \epsilon_2 (1-\epsilon_1) \text{MAX}\{0.01 \delta\rho (|u|+|v|), 2|\rho U|\}_{i+1/2}$$

$$\begin{aligned} \epsilon_1 &= \text{MAX}(\lambda, \text{MIN}(1.0, 25v_{i+1/2})) \\ \epsilon_2 &= 0.015 \\ v_{i+1/2} &= \text{MAX}(v_i, v_{i+1}) \\ \gamma_i &= |p_{i+1} - 2p_i + p_{i-1}| / (p_{i+1} + 2p_i + p_{i-1}) \end{aligned}$$

In the above formulations, unity λ corresponds to a full upwind differencing scheme for the momentum and energy equations and vanishing λ corresponds to a central differencing scheme for the convective terms in smooth regions. δ stands for the local flow area.

Viscous fluxes and source terms are discretized using second order central difference approximation. A pressure based predictor plus multi-corrector solution method is employed so that flow over a wide speed range can be analyzed. The basic idea of this pressure based method is to perform corrections for the pressure and velocity fields by solving a pressure correction equation so that velocity/pressure coupling is enforced, based on the continuity constraint at the end of each iteration. Details of the present numerical methodology is given by ref. 1-2.

Computational Grid Generation

GENIE++ [3-4], a general purpose three-dimensional grid generation package, was used to generate the grid for this investigation. In addition, an intersection technique was developed to model the piston-cylinder interface. To simplify the geometry, the diameter of the cylinder is kept constant. H-type grid was then chosen to model the entire flow geometry. The main cylinder and piston was cut into half at the plane of symmetry to reduce the size of the domain. Five-block zonal grid was generated: the inlet pipe, the lower part of the main cylinder, and the remaining three blocks that describe the upper part of the main cylinder. The final grid is shown in Fig. 3. The total number of grid points was 91,612.

Boundary & Initial Conditions

Due to symmetry, the computational domain occupies only the front half of the SRV. Fully developed velocity and turbulence profiles were used at the inlet and mass conservation was enforced at the exit. The total condition was held at the inlet. Adiabatic condition was applied to all solid walls. Flow properties at the wall, symmetry plane and exit boundary were extrapolated from those of the interior domain. Quiescent environment was used to initialize the flow field.

No-slip condition was imposed on the solid wall boundary and tangency condition was applied to the symmetry plane. A modified wall function approach is employed to provide near-wall resolution

which is less sensitive to the near-wall grid spacing. This is achieved by incorporating a universal velocity profile [5]. That is,

$$u^* = \ln [(y^* + 11)^{4.02} / (y^* - 7.37y^* + 83.3)^{0.79}] + 5.63 \tan^{-1}(0.12y^* - 0.441) - 3.81$$

where $y^* = y u^* \rho / \mu$ and $u^* = (\tau_w / \rho)^{1/2}$. y_a denotes the distance between the near wall point and the solid wall and τ_w is the shear stress on the wall. This universal velocity profile provides a smooth transition between Logarithmic law-of-the-wall and linear viscous sublayer velocity distributions.

Results and Discussions

The mishap was assumed to happen at a fixed time on the timeline and a fixed clearance of valve opening was assumed. It is therefore a quasi-steady calculation and the initial temperature and pressure of the inlet were assumed to be 100 deg. R and 5500 psi, respectively. The computed temperature gradient (not shown) near the piston/nozzle area was low. The computed temperature ranged from 830 deg. R to 1050 deg. R. It is therefore decided that aerodynamic heating was not the cause of the fire, rather the frictional force that occurred between the piston and the sleeve could have been the culprit.

It was theorized by the investigation team that the LOX pressurization valve opened in an uncontrolled manner and increased the pressure in the LOX tank from about 20 psi to about 5500 psi. The most probable reason that the pressurization valve opened was the servo valve that controls the position of the plug head of the pressurization valve malfunctioned. The SRV then discharged, as designed, due to the line pressure reaching 5500 psi.

Ignition must have occurred due to frictional heating between the piston and sleeve of the main valve body. From the analyses of the investigation team, the frictional heating was mostly likely caused by a combination of resonant chatter and low frequency oscillation due to water hammer. In this study, a separate calculation using a thermodynamic code [6] was also performed. The result indicated that under the very conditions, a combination of elemental iron and pure oxygen would have burned and produced an adiabatic flame temperature as high as 6,800 deg. R. The frictional heating could provide a initial spark, that would initiated a local combustion. The long residence time of the vortices that surrounded the piston would have created an environment that could have sustained the flame and allowed it to propagate. Eventually the propagated flame expanded and swallowed the whole SRV.

To aggravate the matter, the melting point of iron is 3,280

deg. R and the boiling point of iron is 5,423 deg. R. The adiabatic flame temperature certainly exceeded both the melting point and boiling point. A cloud of melted and vaporized metal particles could have been resulted and engulfed by the flame.

Fig. 4 shows the fluid particle around the piston. The vortices evidenced by those particle traces, combined with the flow recirculation, agreed with the erosion pattern of the damaged hardware (Fig. 2).

Conclusion

A three-dimensional CFD calculation was performed to investigate the flow anomaly occurred involving a high pressure SRV. The predicted flow pattern, combined with other analyses, agreed with the erosion pattern of the damaged hardware. A possible mishap scenario may be proposed: the mishap was caused by the malfunctioning of a pressurization valve which caused the discharge of high pressure fluid into the SRV; a spark was initiated by the frictional force, and the recirculated flow pattern enhanced the flame holding and the eventual flame propagation.

REFERENCES

1. Wang, T.-S., "Numerical Study of the Transient Nozzle Flow Separation of Liquid Rocket Engines," Computational Fluid Dynamics Journal, Vol.1, No.3, Oct. 1992, pp. 305-314.
2. Wang, T.-S. and Chen Y.-S., "Unified Navier-Stokes Flowfield and Performance Analysis of Liquid Rocket Engines," Journal of Propulsion and Power, Vol. 9, No. 5, Sept.-Oct. 1993, pp.678-685.
3. Soni, B.K., "GENIE: Generation of Computational Grids for Internal-External Flow Configurations," Numerical Grid Generation in Computational Fluid Dynamics, S. Sengupta, J. Hauser, P.R. Eiseman, J.F. Thompson (eds.), Pineridge Press, 1988.
4. Soni, B.K., Thompson, J.F., Stokes, M., and Shih, M.H., "GENIE++, EAGLEView, and TIGER: General and Special Purpose Graphically Interactive Grid Systems," AIAA paper 92-0071, Jan. 1992.
5. Liakopoulos, A., "Explicit Representations of the Complete Velocity Profile in a Turbulent Boundary Layer," AIAA JOURNAL, Vol. 22, No. 6, Jan. 1984, pp. 844-846.
6. Svehla, R.A., and McBride, B.J., "FORTRAN IV Computer Program for Calculation of Thermodynamic and Transport Properties of Complex Chemical Systems," NASA TN D-7056, 1973.

Figure Captions:

Fig. 1 A schematic of the general arrangement of the pilot operated safety relieve valves

Fig. 2 The damaged valve body

Fig. 3 The computational grid

Fig. 4 The particle traces around the piston (front view)

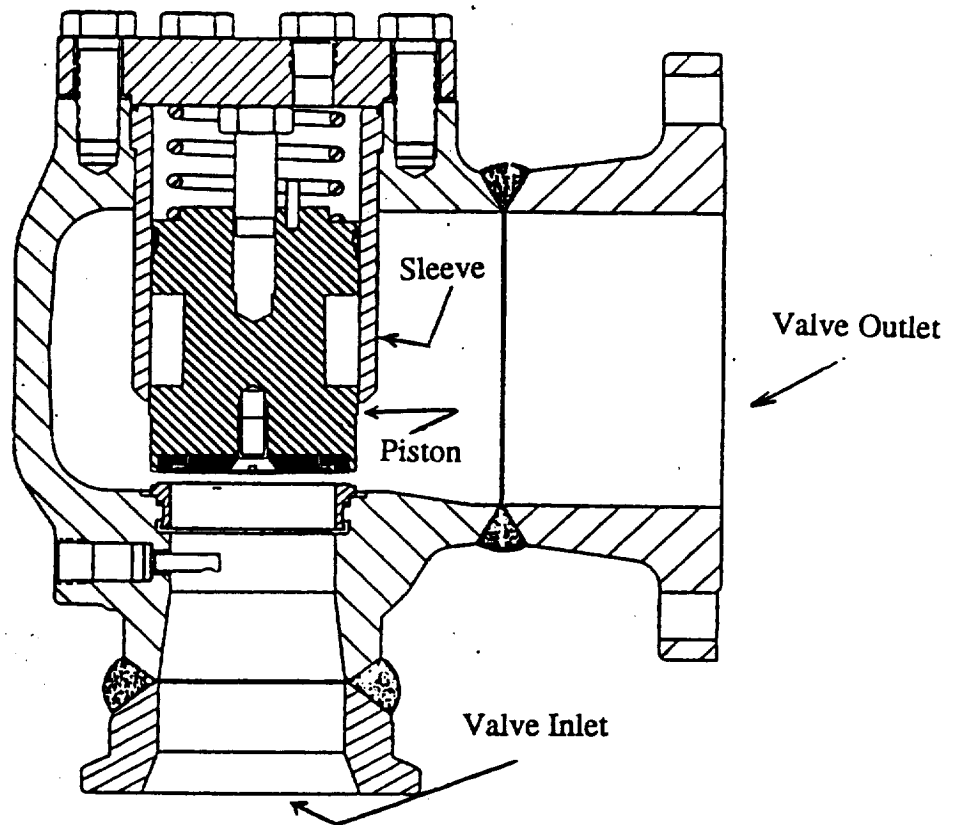


Fig. 1 A schematic of the general arrangement of the pilot operated safety relieve valves



Fig. 2 The damaged valve body

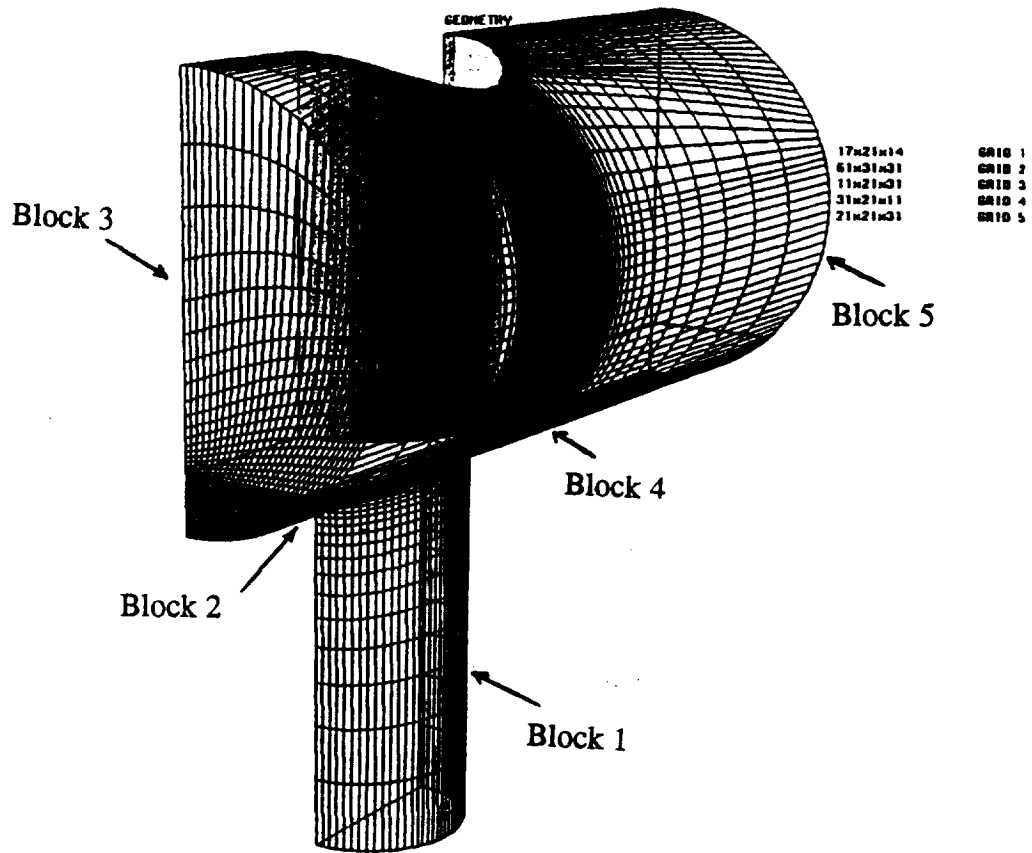


Fig. 3 The computational grid

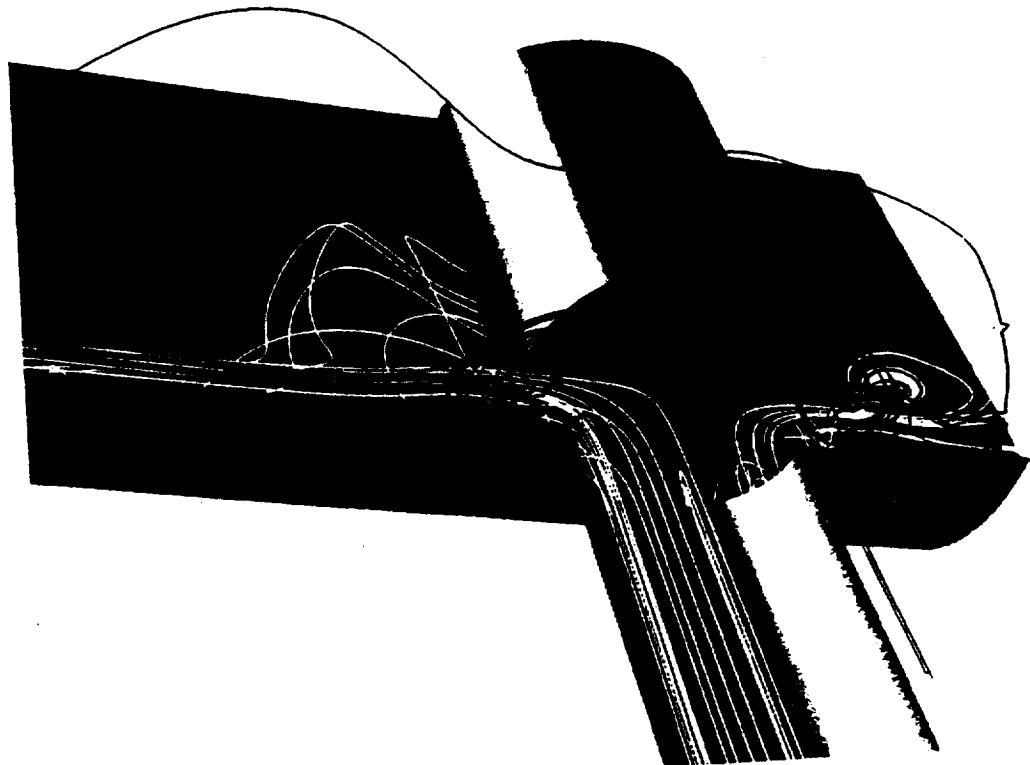


Fig. 4 The particle traces around the piston